Joint SCSP-LROM: A novel approach to detect Cerebrovascular Anomalies from EEG signals

Debojyoti Seth

It has always been a big challenge to identify subtle changes in Electroencephalogram (EEG) signals. Minor differences often lead to vital decisions, for example, which grade a certain tumour belong to or whether a haemorrhage can result in benign blood clots or cancerous ones. In recent studies on brain computer interfaces (BCIs), one of the biggest challenges is recovering maximum information for realistic predictions. In order to choose EEG channels with highest accuracy, a novel notion of including sparsity in a modified common spatial pattern (CSP) algorithm is introduced here. Being influenced by the existing concept of compressed sensing, an optimization model is also developed alongside to recover the cosparse signal and retain maximum information. The state-of-the-art Joint Sparsity Induced Modified Common Spatial Pattern Algorithm and Low Rank Optimization Model (SCSP-LROM) developed here is capable of identifying and describing tumours and lesions in great detail at an overall accuracy of 96.3%.

Introduction: Electroencephalogram (EEG) is one of the most commonly discussed method among brain computer interfaces (BCIs) [1]. EEG has gained more popularity over similar modalities like frequency magnetic resonance imaging (fMRI) or functional near infrared spectroscopy (fNRIS) for its highly non-invasive nature, simpler testing facilities and easier budget-friendly market availability [2]. However, EEG poses certain challenges till date and somehow restricts the ability to safely predict cerebrovascular anomalies, like, grade of a tumour or the type of a haemorrhage which often leads the doctors to recommend further complex investigations to determine the extent of illness of a particular patient. Interestingly, most EEG researches restricted its scope to movement [1, 4, 10] or epilepsy detection [5, 6, 9]. It has always been a great challenge to efficiently select EEG channels, retrieve necessary information and make major decisions solely based on EEG output [3].

Various channel selection methods are proposed and techniques are adapted since early 2000's. Support Vector Machines (SVMs) are capable of recursive elimination of the least contributing channels [7]. SVM is solely dependent on individual performance of certain classifiers to evaluate the quality of a set of features. Thus, it proved its effectivity in solving simple problems like classifying specific classes of epilepsy. But complex problems like brain haemorrhages at particular location can never be identified on losing data in an uncontrolled fashion by the process of eliminating the least contributor from the first iteration. The process of ranking the channels depending solely on Mutual Information (MI) between the class labels do overcome the problem partially as they are independent of classifiers [8] and is capable of ranking channels individually but fails to consider channel correlations. So, data flow among the cerebrovascular lobes is mostly ignored. Although Convolutional Neural Networks (CNN) helps in automated selections of EEG channels [9] and is quite a remarkable development over traditional approaches, the accuracy of data sorting and classification is significantly low. Further improvement in concepts is observed by the introduction of common spatial pattern (CSP) algorithm which leads to direct channel selection based on CSP coefficients without deriving features for each channel [10]. CSP is often found to be extremely sensitive to the slightest contaminants and not so versatile in adapting to complex ever-changing biomedical data. Despite rigorous efforts of optimally extracting maximum information from EEG channels and predicting symptoms remotely, the way to do so has always remained a challenge.

A novel notion of sparsity induced modified CSP (SCSP) is discussed to conduct selection of EEG channels optimally. The algorithm sparsifies the spatial filters and this in turn helps in reducing the number of channels significantly. While visualizing the SCSP algorithm as a convex optimization problem, the limitation of rapid loss of multi-channel information hinted to search for new avenues. Hence, a low rank optimization model (LROM) is developed to follow the sparse CSP in order to revoke the beneficial artifacts which often turns out to be essential to address complex and realistic scenarios like benignity of an apparent malignant tumour. Here, a state of the art joint SCSP-LROM model is developed and tested on nearly 200 Gigabytes of EEG data and have established an average accuracy of 95.2% on predictions related to unhealthy datasets and 97.8% on predictions related to healthy datasets.

Sparsity induced Modified CSP algorithm: Ideally speaking, if a hypothetical EEG setup has only two channels, a standard CSP algorithm will aim to distinguish by extensively altering the variances, maximizing the variance of one class of data while minimizing the other. Assuming there are n EEG channels each generating s observables and $X \in \mathbb{R}^{n\times s}$ represents the EEG of any single trial in a multi-channel setup, a CSP matrix W^{-1} generates a Z, spatially filtered by W on X i.e., $Z = WX$. Let us assume, for a particular test, ϱ classes of EEG data are required and the covariance matrices (covmat) of the ϱ classes are given by, $C_1, C_2, \dots, C_\varrho$ where for any class i, $C_i = \frac{X_i X_i^T}{\text{trace}(X_i X_i^T)}$. Defining F as the matrix of normalized eigenvectors and ψ as the eigen value matrix, the composite covmat and EVD can be derived as $\mathbb{C}= \sum_{i=1}^{\varrho} C_i = F\psi F^T$. Next, using CNN, two pairs are chosen randomly from the tuple of ϱ covariance matrices and the process is repeated until the required precision is achieved. The uniqueness of the Modified CSP algorithm described here is that any two covmat, namely, C_1 and C_2 are so uniquely chosen that they discuss two distinct characteristics and the next iteration delves further in two deeper pronounced features between the already labelled feature maps. With such an approach on optimized confusion matrices, the feature map can be extensively labelled and isolated, and the region of interest (ROI) can be identified in just a few iterations at an impressively high precision rate. Furthermore, the CSP algorithm formulation as a quadratic programming problem help to include the sparsity in it in terms of introducing a regularization parameter, $r \in [0,1]$ to control the numbers of channels removed. In the first stage, instead of l_0 norm, the $\frac{l_1}{l_2}$ norm is considered for sparsity introduction primarily because it can be safely considered as a non-sparsity measure (mostly, minimal data is ignored and those channels are also highly affected by gaussian white noise and of no use) although, it is capable of including necessary attributes which is generally expected when sparsity is fully included without the regularization parameter. The sparsity induced CSP algorithm for any two covmat C_1 and C_2 is proposed as follows:

$$\min_{w_i}(1-r)\left[\sum_{i=1}^{m} w_i C_2 w_i^T + \sum_{i=m+1}^{2m} w_i C_1 w_i^T\right] + r\sum_{i=1}^{2m}\frac{||w_i||_1}{||w_i||_2}$$
$$\text{subject to: } w_i(C_1+C_2)-1 \le 0,\ w_i(C_1+C_2)=0,\ i=\{1,2,\dots,2m\} \quad (1)$$

Efficient Channel Selection: The regularization parameter, r plays a significant role in controlling the extent of channels selection and corresponding accuracy, hence needs to be wisely chosen. Even slight change in the regularization parameter can lead to drastic changes in the system performance and can lead to erroneous predictions and even lead the CNN unit to repetitive loops without even getting closer to the required precision. Channel ranking is observed pairwise from both motor imagery areas. First, two sparse spatial filters corresponding to two motor imagery tasks are obtained on solving Eq. (1) with $m = 1$. A concept of ranking is generated which yields the top-ranked channels for each task efficiently.

Let CH represent the channel ranks and $ch(|w_{1,i}|)$ represent the i-th best channel of any motor imagery task 1. As considered pairwise, after first iteration, let p and q represent the total number of remaining channels in the first and second spatial filters. Also, $l = \min(p, q)$. The overall ranking is performed as follows:

$$\begin{aligned} CH_{2i-1} &= ch\left[\max\left(|w_{1,i}||w_{2,i}|\right)\right]\ i \in [1,l] \\ CH_{2i} &= ch\left[\min\left(|w_{1,i}||w_{2,i}|\right)\right]\ i \in [1,l] \\ If\ p > l, CH_{l+i} &= ch\left(|w_{1,i}|\right)\ i \in [1+l,p] \\ else, \quad CH_{l+i} &= ch\left(|w_{2,i}|\right)\ i \in [1+l,q] \end{aligned} \quad (2)$$

Solution to the optimization problem: Like any convex optimization problems, the novel sparsity induced Modified CSP algorithm introduced in Eq. (1) can have multiple solutions, one of which is elaborated hereafter.

Let us define $f(x)$ and $c_i(x)$ as follows:

$$f(x) = (1-r)\left[\sum_{i=1}^{m} w_i C_2 w_i^T + \sum_{i=m+1}^{2m} w_i C_1 w_i^T\right] + r\sum_{i=1}^{2m}\frac{||w_i||_1}{||w_i||_2}$$
$$c_i(x) = 1 - w_i(C_1 + C_2) \geq 0 \; \forall \; i \in \{1,2,\dots,2m\},$$
$$x \in \mathbb{R}^{2m},\; f: \mathbb{R}^{2m} \to \mathbb{R},\; c_i: \mathbb{R}^{2m} \to \mathbb{R} \tag{3}$$

One of the most common approach is adapting the primal dual methods to solve Eq. (3). For that, a logarithmic barrier function is developed. $B(x,\mu)$ is the barrier function of Eq. (3) and interestingly, as the barrier parameter μ (a small positive scalar) approaches zero, $B(x,\mu)$ converges to the optimal solution of $f(x)$.

$$B(x,\mu) = f(x) - \mu\sum_{i=1}^{2m}\log\left(c_i(x)\right) \tag{4}$$

Gradient of the barrier function, g_B, is derived as:

$$g_B = g - \mu\sum_{i=1}^{2m}\frac{1}{c_i(x)}\nabla c_i(x) \tag{5}$$

where g is the gradient of the original function $f(x)$ and $\nabla c_i(x)$ is the gradient of the function $c_i(x)$. In addition to the primal variable x, a dual variable $\lambda \in \mathbb{R}^{2m}$ is introduced as follows:

$$c_i(x)\lambda_i = \mu,\; \forall\; i \in \{1,2,\dots,2m\} \tag{6}$$

The objective is to find the (x_μ, λ_μ) for which $g_B = 0$. It can be derived as:

$$g - A^T\lambda = 0 \tag{7}$$

where matrix A is the Jacobian. Intuitively speaking, gradient of $f(x)$ should be contained in a subspace which can only be formed on spanning the constraint's gradients. The extreme cases are really small values of μ. There are two possible explanations for that. Either the solution merges with the boundary or the gradient projection is nullified. From Eq. (6) and Eq. (7), on applying Newton-Raphson Method an equation for (x,λ) is derived. For H as the Hessian of matrix $B(x,\mu)$, D as the diagonal matrix of λ and C as the diagonal matrix with $C_{jj} = c_j(x)$, update (p_x, p_λ):

$$\begin{bmatrix} H & -A^T \\ DA & C \end{bmatrix}\begin{bmatrix} p_x \\ p_\lambda \end{bmatrix} = \begin{bmatrix} -g + A^T\lambda \\ \mu - C\lambda \end{bmatrix} \tag{8}$$

The condition $\lambda \geq 0$ must be enforced in each step and it is possible if it updates (x,λ) at every iteration for an appropriate learning rate α, as,

$$(x,\lambda) \to (x + \alpha p_x, \lambda + \alpha p_\lambda) \tag{9}$$

Low Rank Optimization Model: It is worth mentioning that given the dynamic nature of EEG signals, the sparsity induced modified CSP model is capable of analysing healthy datasets. However, for carcinogenic/lesions data at input, prediction accuracy has significantly improved on passing the sparsity induced modified CSP model output through the low rank optimization model. The semi-classified output from the previous stage is fed in here. An optimization model is developed for recovering cosparse signals to compensate even minor losses from the sparse modified CSP algorithm. The existing concept of compressed sensing (CS) has been utilized [10]. The low rank optimization model is developed on successfully implementing both the l_0 norm and $\text{Schatten} - 0$ norm on the stacked up multichannel data X. The $\Omega \in \mathbb{R}^{Q\times N}$ denotes the cosparse representation matrix. Q basically, represents the analysis dictionary and the second-order difference matrix is chosen for the role.

$$\underset{\mathrm{X}}{min}||vec(\Omega\mathrm{X})||_0 + ||\mathrm{X}||_{\text{Schatten}-0} \text{ subject to } Y = \Phi\mathrm{X} \tag{10}$$

Convex Relaxation: The easiest approach to solve Eq. (10) is first converting the zeroth norms to first norms. What taxicab norm and nuclear norm does is very intuitive. Taxicab norm (l_1 norm) adds up the singular values but nuclear norm adds up the absolute values of entries. For the relaxation, l_1 norm can be converted to linear programming, however the $\text{Schatten} - 1$ norm has to be dealt together with the approximation constraints. Hence, they both are replaced by matrix inequalities. For the conversion and finally the convex relaxation, let us define two variables $e, \mathbb{f} \geq 0$:

$$\underset{\mathrm{X},e>0,\mathbb{f}\geq 0}{minimize}\, 1^T e + \mathbb{f} \text{ subject to } Y = \Phi\mathrm{X}, ||\mathrm{X}||_* \leq \mathbb{f}, -e \prec vec(\Omega\mathrm{X}) \prec e \tag{11}$$

Thus, the optimization model is derived as follows:

$$\underset{\mathrm{X},e>0,\mathbb{f}\geq 0}{minimize}\, 1^T e + \mathbb{f}$$
$$\text{subject to } Y = \Phi\mathrm{X},\; -e \prec vec(\Omega\mathrm{X}) \prec e,$$
$$\begin{bmatrix} \mathrm{A} & \mathrm{X} \\ \mathrm{X}^T & \mathrm{B} \end{bmatrix} \geq 0,\; Tr(\mathrm{A}) + Tr(\mathrm{B}) < \mathbb{f} \tag{12}$$

Here, $\mathrm{A} = \mathrm{A}^T$ and $\mathrm{B} = \mathrm{B}^T$. Eq. (12) represents a semi definite programming (SDP) and is solved by primal-dual Interior Point Methods.

Experiments: 40,000 labelled (based on gender, age and clinical history) EEG recordings from an online database, namely, TUH EEG Corpus [11] is used for all experimentations. Keeping legal and ethical barriers in mind, no clinical trial has been conducted to test existing algorithms [9, 10] and proposed ones for monitoring predictability, feature map generations or accuracy comparisons.

Discussion: In a brief context, the utility and accuracy of the proposed method is discussed.

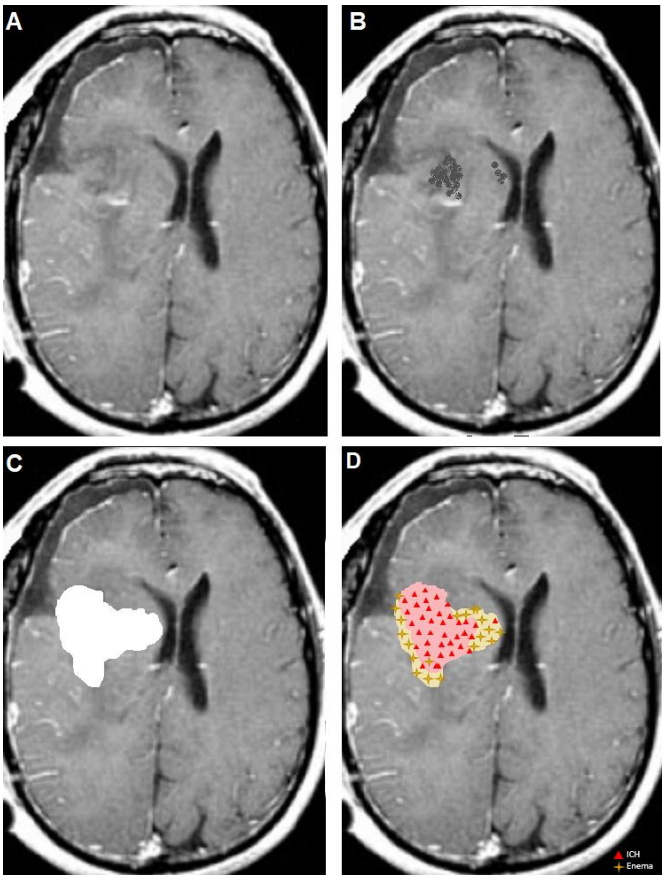

Fig. 1 *Haemorrhage and Edema detection based on A. Raw Input, B. Modified CSP, C. Sparsity induced modified CSP (SCSP) and D. Joint SCSP-LROM*

The visualization platform with the raw input, Fig. 1.A, shows some fuzziness in the left frontal lobe which is somewhat narrowed down to a region of interest (ROI) in Fig. 1.B. The optimal value of regularization parameter $r \in \mathbb{R} = \{0.01, 0.02, \dots, 0.99\}$ of Eq. (1) helped isolating the total affected area (possibly haemorrhage/carcinoma) in Fig. 1.C which is further classified, labelled and isolated in Fig. 1.D using Joint SCSP-LROM. The novel joint SCSP-LROM model has proved its capability on discriminating between haemorrhage and edema and precisely isolating and labelling the ROI. The index 'triangles' identifies a deep intracerebral haemorrhage (ICH) between the left frontal and parietal lobe and the observation is further confirmed by the growth of edema (indexed as 'stars') surrounding it which is encroaching towards the adjacent lateral ventricle.

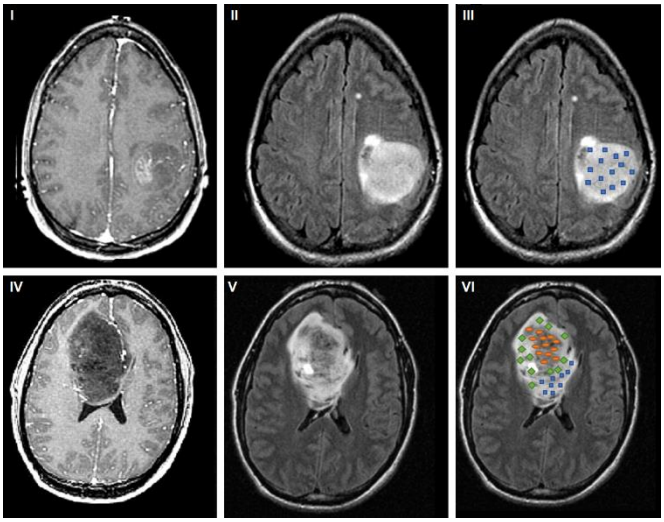

Fig. 2 *Brain tumour detection and classification based on I, IV. Modified CSP, II, V. Sparsity induced modified CSP (SCSP) and III, VI. Joint SCSP-LROM*

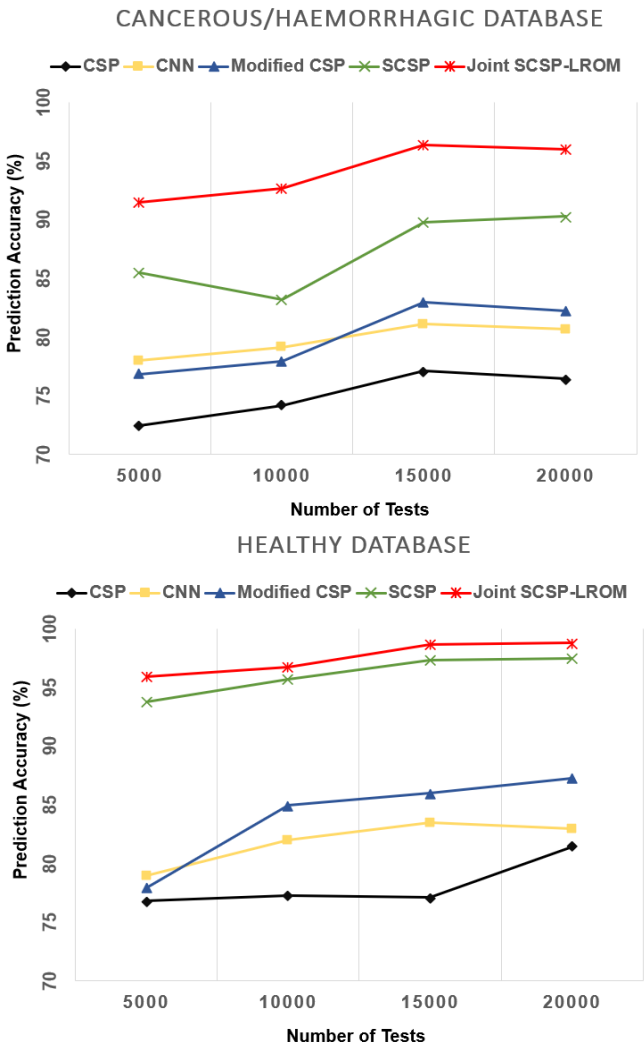

Fig. 3 *Accuracy Comparison for Predictions through CSP, CNN, Modified CSP & Joint SCSP-LROM on healthy and unhealthy database*

Fig. 2 proves the ability of the joint SCSP-LROM model to predict the nature of an abnormal mass (whether the tumour is benign/carcinogenic) and also label the grade of the growth and predict the extent to which the mass is spreading. Fig. 2.III, identifies the mass between lower right parietal and occipital lobe as a grade-3 astrocytoma. The density of the growth is analysed thoroughly. Fig. 2.VI identifies the mass located mostly between both the frontal lobes and largely affecting the lateral ventricle. It is labelled as a grade-2 astrocytoma. In this case, the lowest density and more of a forming stage of the tumour is observed on the lateral ventricle (indexed by 'circles') which is closely followed by slightly denser vicinities around the ventricles (indexed by 'diamonds'). However, the junction between both the frontal and parietal lobes has the highest density of the mass (indexed, 'squares'). A deeper analysis on Fig 2.I-III depicts the fact that although it is a grade-3 astrocytoma, it is contained and spreading much slower that the grade-2 astrocytoma in Fig 2.IV-VI. Numerically speaking, the grade-2 astrocytoma is increasing its mass at a surprising rate of 21.4% compared to the only 8.2% of the grade-3 astrocytoma and the latter is expected to affect the brain its associated to, 16% less than the earlier.

Conclusion: The state of the art SCSP-LROM described here is capable of identifying cerebrovascular anomalies to extensive details, like, confirming a stage of a cancer or distinguishing between various classes of haemorrhages and predicting its possible growth to an overall accuracy of 96.3%. Fig. 3 compares the accuracy of prediction for healthy and infected (cancerous/lesions) datasets over a dedicated run on 20,000 tests. Based on the comparative analysis, it is well established that both SCSP or the novel Joint SCSP-LROM is capable of making predictions far better than recent trendy models, like, deep CNNs or CSPs. A mean accuracy of 95.2% on predictions related to unhealthy datasets and 97.8% on predictions related to healthy datasets is observed. Future plans include testing the model for different pathological investigations and designing a common Internet of Things based framework for easier data handling.

Debojyoti Seth (Department of Computer Science, University of New Hampshire, Durham, NH 03824, United States)
E-mail: seth_d@ieee.org

References

1. Norman, Sumner L., et al. 'Movement anticipation and EEG: implications for BCI-contingent robot therapy', *IEEE Transactions on Neural Systems and Rehabilitation Engineering*, 2016, 24, 8, pp. 911-919, doi: 10.1109/TNSRE.2016.2528167
2. Seth, Debojyoti, et al. 'Brain computer interfacing: A spectrum estimation based neurophysiological signal interpretation', *IEEE International Conference on Signal Processing and Integrated Networks*, 2017, pp. 534-539, doi: 10.1109/SPIN.2017.8050008
3. Baig, MZ, et al. 'Filtering techniques for channel selection in motor imagery EEG applications: a survey', *Artificial Intelligence Review*, 2020, 53, 2, pp. 1207-1232, doi: 10.1007/s10462-019-09694-8
4. Ang, Kai Keng, et al. 'EEG-based strategies to detect motor imagery for control and rehabilitation', *IEEE Transactions on Neural Systems and Rehabilitation Engineering*, 2016, 25, 4, pp. 392-401, doi: 10.1109/TNSRE.2016.2646763
5. Ullah, Ihsan, et al. 'An automated system for epilepsy detection using EEG brain signals based on deep learning approach', *Expert Systems with Applications*, 2018, 107, pp. 61-71, doi: 10.1016/j.eswa.2018.04.021
6. Tatum, W. O., et al. 'Clinical utility of EEG in diagnosing and monitoring epilepsy in adults', *Clinical Neurophysiology*, 2018, 129, 5, pp. 1056-1082, doi: 10.1016/j.clinph.2018.01.019
7. Saccá, Valeria, et al. 'On the classification of EEG signal by using an SVM based algorithm', *Multidisciplinary Approaches to Neural Computing, Springer, Cham*, 2018, 69, pp. 271-278, doi: 10.1007/978-3-319-56904-8_26
8. Meng, Jianjun, et al. 'Simultaneously optimizing spatial spectral features based on mutual information for EEG classification', *IEEE transactions on biomedical engineering*, 2014, 62, 1, pp. 227-240, doi: 10.1109/TBME.2014.2345458
9. Zhou, Mengni, et al. 'Epileptic seizure detection based on EEG signals and CNN', *Frontiers in Neuroinformatics*, 2018, 12, 95, pp. 1-14, doi: 10.3389/fninf.2018.00095
10. Yu, Hongbin, et al. 'A General Common Spatial Patterns for EEG Analysis With Applications to Vigilance Detection', *IEEE Access*, 2019, 7, pp. 111102-111114, doi: 10.1109/ACCESS.2019.2934519
11. Harati, A., et al. 'The TUH EEG CORPUS: A big data resource for automated EEG interpretation', *2014 IEEE Signal Processing in Medicine and Biology Symposium*, 2014, pp. 1-5, doi: 10.1109/SPMB.2014.7002953
Available online: https://www.isip.piconepress.com/projects/tuh_eeg/ (Homepage). Last accessed: September 15, 2020.